

**REMOTE SENSING OF GRANITOID ROCKS:
IMAGE ELABORATION AND SPECTRAL SIGNATURES.
CASE STUDIES ON THE MOROCCO CALC-ALKALINE AND HIMALAYAN
PERALUMINOSE GRANITOIDS**

LUCA BERTOLDI

Dipartimento di Geoscienze, Università di Padova, Via Gradenigo 6, 35131 Padova

INTRODUCTION

The aim of this study is to characterize the spectral signatures in VNIR-SWIR-TIR wavelength regions of granitoid rocks and to find methods to discern them in remote multi-hyperspectral acquisitions (primarily ASTER data and secondarily PROBA and HYPERON data). For this reason some plutons in different geological context have been taken into account. Since some of them have a still unclear genesis and evolution, we also performed a series of petrographic, geochronological, and geochemical analysis. Therefore, the research has been subdivided into different arguments using a multidisciplinary approach that aims, at its final stage, to clarify the origin, the evolution, and the remote sensing discrimination of the tertiary Himalayan plutons.

Hence, the research has been focused to the following granitoid rocks cropping out in the following different environments: i) Anti-Atlas, Morocco, Ediacarian, and Cryogenian plutons; ii) Sardo-Corse Ercinian batholiths; iii) Himalaya Tertiary plutons.

The remote sensing and laboratory studies on Anti-Atlas and Corse granites have been preparatory to the detection and mapping of granitoids in the extreme terrains of the vegetated and roughly profiled Southern Himalayan Belt.

The work-flow started from image raw data pre-processing and continued by comparing satellite, field and laboratory data. Remote sensing elaborations point out that the masking technique adopted to isolate rocky pixels is of fundamental importance to perform further analyses. An integration of density-sliced and false colours composite images of Band Ratio, Relative Absorption Deep and Principal Component Analysis allowed us to generate geological map that highlights different granitoid bodies.

Petrographic studies on the samples were useful to determine the mineralogy of the studied lithologies and hence to interpret and compare the laboratory and satellite spectral data.

One of the results is the discovery of a new leuco-granite pluton (Buraburi Granite) and the surrounding host rocks in the Dolpo region, a remote Nepalese region.

In conclusion, it has been demonstrated the effectiveness of the innovative approach adopted that considers the absorption features of particular lichens species (acidophilic) as a proxy in the detection of granitoid rocks. Furthermore, since peraluminous granitoids, as those from Buraburi, have a considerable Al_2O_3 bulk-rock content, the muscovite Al-OH absorption peaks centred in the 6th ASTER band were also considered an important parameter for their detection.

Finally, the proposed methods have a great potential for lithological mapping in vegetated and rough terrains with climatic and geological conditions similar to those of the Southern Himalayan belt.

ASTER DATA AND PRE-PROCESSING TECHNIQUE

ASTER is a multispectral (14 bands) system that includes three instruments: a visible-near infrared sub-system (VNIR) allowing radiometric measurements and stereo-acquisition, a short-wave infrared (SWIR) radiometer, and a thermal infrared (TIR) radiometer (Fujisada, 1995; Abrams, 2000).

The remote sensing analyses were carried out using the IDL-ENVI[®] and the ESRI-ARCGIS[®] software on ASTER L1B and L1A data.

The Level-1B data product can be generated by applying radiometric coefficients to perform the radiometric calibration and geometric resampling of Level-1A data. In this way the DN (Digital Number) becomes a “radiance at sensor” data ($W/m^2/sr/\mu m$).

The following pre-processing steps were applied on Level-1B:

- 1) correction of the SWIR bands crosstalk effect;
- 2) DEM extraction using the stereoscopic images: Band 3N and Band 3B;
- 3) SWIR and TIR bands resampling at 15m/pixel;
- 4) correction of SWIR-VNIR geographic shift;
- 5) orthorectification;
- 6) conversion of the VNIR-SWIR bands from “radiance at sensor” to “ground reflectance” and TIR bands into “ground emittances” (atmospheric correction);
- 7) correction of the topographic effects using SRTM data conveniently resampled and interpolated, preferably using a non Lambertian method, such as the Minnaert Correction or more complex Teillet and C-correction methods that use empirical-statistical approaches (Riano *et al.*, 2003; Twele & Erasmi, 2005; Nikolakopoulos *et al.*, 2006).

ASTER PROCESSING

Detailed lithological discrimination, especially near or above particular objectives like vegetated and topographically rough areas, requires advanced digital image processing techniques. A good approach consists on masking non bedrock pixels through a classification based on specified filtering criteria that exclude water, snow, vegetation and clouds. Looking at the distribution of rocky pixel reflectance values in a multidimensional visualizer we were able to cluster them in few end-members, each one with a particular spectral signature. The comparison between end-member spectral signatures and granitoid signatures previously collected in other ASTER images (Himalaya, Corsica, Morocco) allowed us the distinction of granite-likely signatures. A SAM (Spectral Angle Mapper) and a MLL (Maximum Likelihood) classification with such signatures helped us to find the Buraburi Granite (BG) and to derive its real spectral signature on the ASTER data. In order to refine the pluton boundary, on the basis of the study of Yamaguchi & Naito (2003), Ninomiya *et al.* (2005), Rowan *et al.* (2005), Massironi *et al.* (2008) and to look at the end-member spectral features of ASTER data, we have chosen several mineral-rock indices and characteristic band operation. The 5*7/6 operation and the 5/6 and 7/6 bands ratios underline the spectral shape in the middle of SWIR sensor, a zone affected by the characteristic Al-OH and OH adsorption peaks in muscovite, whereas the 5/4 bands ratio highlights the Fe-OH vibrational absorption peaks in Fe-silicates like biotite and inosilicates.

The thermal bands have proved to be useful over arid and relatively flat terrain target (Morocco) but in the high relief of the Himalayan studied zone the emissivity is more strongly affected by the topography than by the mineralogical composition of the investigated materials.

LABORATORY SPECTRAL SIGNATURES

In order to define the spectral separability of the involved lithologies (*i.e.* granitoid, gneisses, and limestone) and their minerals, we analyzed the high resolution laboratory spectral signatures of rocks and minerals from the ASTER Spectral Library version 2.0 (Baldrige *et al.*, 2009). This library includes contributions from the Jet Propulsion Laboratory (JPL), Johns Hopkins University (JHU), and the United States Geological Survey (USGS) (Christensen *et al.*, 2000; Clark *et al.*, 1990, 2007). Furthermore, forty-five samples of granitoid rocks collected in the field, were analyzed in the VIS/SWIR spectral range at the DEI (Department of Information Engineering - University of Padova) using the VARIAN-CARY5000[®] spectrophotometer. In particular the spectral signatures were collected using an Integrating Sphere in the wavelength range between 350 nm and 2500 nm with a 1 nm sampling step.

The high-resolution spectral signatures were re-sampled simulating the ASTER bands filter. This transformation reduces considerably the ability to discern different spectral signatures, obtaining 9 bands from the 2150 laboratory “bands”.

CASE STUDIES RESULTS

Study of East Anti-Atlas (Morocco), Ediacarian, and Cryogenian plutons

ASTER data were used to clarify the geological framework of the Precambrian basement in the Saghro massif (eastern Anti-Atlas, Morocco). The Saghro basement is composed of low-grade metasedimentary sequences of the Saghro Group (Cryogenian), intruded by calc-alkaline plutons of late Cryogenian age. These rocks are unconformably covered by volcanic to volcanoclastic series of Ediacarian age that are broadly coeval with the granitoid plutons. All of these units are cut by a complex network of faults associated with hydrothermal fluid flows, which developed during, and shortly after, the emplacement of the volcanic rocks (Massironi *et al.*, 2008). The geological mapping of the Precambrian units was challenging in particular for the Ediacarian granitoid bodies, because they are characterized by very similar compositions and by a widespread desert varnish coating. For this reason, a two-stage approach has been adopted. In the first step, false color composites, band ratios, and principal components analyses on visible and near infrared (VNIR) and shortwave infrared (SWIR) bands were chosen and interpreted on the basis of the field and petrographic knowledge of the lithologies, in order to detect major lithological contacts and mineralized faults. In the second step, a major effort was dedicated to the detection of granitoid plutons using both thermal infrared (TIR) and VNIR/SWIR data.

TIR data analysis

Despite their low resolution (90 m), the thermal infrared data are generally considered the most appropriate for identifying granitoid rocks (Sabins, 1996; Drury, 1997) because TIR spectra are only weakly disturbed by the desert varnish, which can have a detectable influence only if dominated by clay minerals (Salisbury & D’Aria, 1992; Christensen & Harrison, 1993).

Therefore, ASTER TIR bands were used to evaluate Reststrahlen and Christiansen effects in the granitoid rocks spectra.

VNIR/SWIR data analysis

Spectral angle mapper (SAM) and supervised maximum-likelihood classifications (MLL) were carried out on VNIR/SWIR data mainly to evaluate their potential for discriminating granitoid rocks. VNIR/SWIR false color composite and ratio images were chosen directly on the basis of the granitoid spectra (derived from both spectrophotometric analyses of samples and selected sites in the ASTER image). Despite their composition, all the outcrops are more or less coated by an arid-environment alteration patina; their mineral composition is a mixture of Fe-, Mn-oxides and clay minerals, similar to many other desert varnish coatings (Hooke *et al.*, 1969). We tried to compare the spectral signatures from the laboratory spectrophotometer with those extracted from Aster satellite multispectral images. The main difference between laboratory and field spectra can be attributed to the opaque minerals of the desert varnish that typically increase the spectral slope at lower wavelengths and mask absorption features at visible and near-infrared rather than at higher wavelengths (Salisbury & D’Aria, 1992).

Moreover, the results have demonstrated the value of ASTER data for geological mapping of basement units, particularly if the processing has been based on a detailed knowledge of the rock mineral assemblages. In addition, the analytical comparison of ASTER TIR and VNIR/SWIR data has demonstrated that the latter are very effective in the distinction of granitoids with very similar silica content, because they can be recognized by secondary effects related to their hydrothermal and surface alterations (K-feldspar kaolinitization, plagioclase saussuritization, replacement of mafic minerals by oxides, inhomogeneous desert varnish coating, and clay/oxide mixtures in different proportions).

Finally, we also performed some statistical methods that allowed to discern the different geological bodies from multispectral-hyperspectral images. Among these methods, the Best Band Ratio (BBR) one showed the best results. BBR algorithm analyzes and compares each band ratio combinations in order to define the best one that evidence one lithology (Massironi *et al.*, 2008).

HIMALAYA TERTIARY PLUTONS

The analysis of ASTER data for lithological mapping of areas with high topographic relief, abundantly covered by vegetation, snow-ice, water bodies and clouds, leads to satisfactory results, when dedicated image pre-processing is applied. In particular, the “rocky” pixels isolation through appropriate masking techniques result unavoidable step for data analysis of such a complex environment. This procedure improves any image visualisation and interpretation by reducing the effect of noisy pixels and limiting the analysis to more suitable areas, as well as facilitates spectra extraction and comparison with laboratory data and, finally, adds strength to the statistical analysis (PCA).

The “rocky” pixels extracted by the masking process can indeed be constituted by non-linear mixing of rocks and lichens signatures. In particular, granitoid rocks of the Higher Himalayan Granitoid form an acid substrate influencing the distribution of acidophilic lichen species which are diagnostic of these rocks. Consequently, the effect of these lichens on rock spectra, along with muscovite absorption bands, can be used as a proxy of the presence of leucogranitic rocks in mid-latitude alpine environment (Fig. 1).

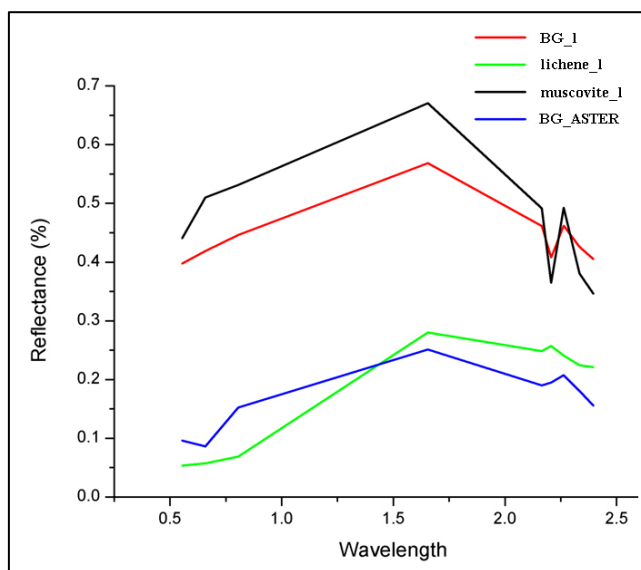


Fig. 1 - Visible-Infrared laboratory and satellite spectra at ASTER resolution. BG_1 (Red line) = BG laboratory fresh rock signature; lichene_1 (green line) = laboratory BG lichens coated surface signature; muscovite_1 (black line) = BG muscovite laboratory signatures; BG_ASTER (blue line) = BG ASTER image average spectral signature.

The image analysis was carried out on SWIR wavelengths using false colour composites of band ratios and PCAs that were studied under the light of this new finding. In fact, image analysis provided the detection and the geological map of a new 110 km² granitoid body (Buraburi Granite - BG) intruding both the HHC and TSS units in the Dolpo region (Fig. 2a, b).

The highlights of AIOH absorption peaks shows encouraging results since muscovite is one of the principal mineral in the peraluminous Himalayan granitoid. In the BG muscovite is often present even in giant crystals (5-10 cm in diameter), contributing to the high Al₂O₃ bulk-rock content, which is an important parameter to classify the granitoid rocks.

Some authors (Law *et al.*, 2006) concluded that Oligo-Miocene leucogranites are restricted to the footwall of the South Tibetan Detachment System (STDS), into the high-grade metamorphic rocks of the Higher Himalayan Crystalline. Despite that, the contact's shape seen in the ASTER image between the BG and the Tibetan Sedimentary Sequence, compromises the

presence of the South Tibetan Detachment System, highlighting a much more complex tectonic evolution and kinematic relations between pluton emplacement and STDS activity.

These findings have substantial implications for the time-extent and even for the existence of the assumed extrusion and/or channel flow mechanisms that would have driven the exhumation of the HHC also in this area.

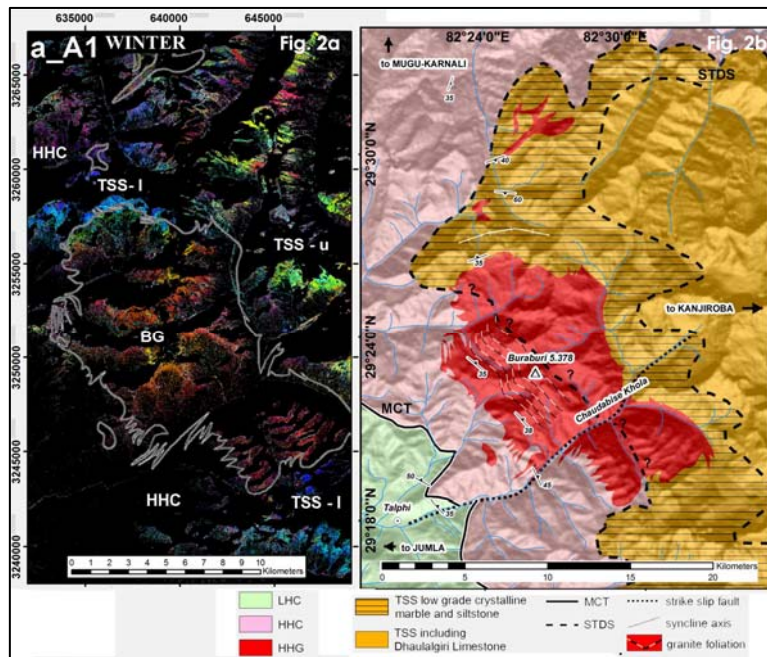


Fig. 2 - a) False colours composites PC 643 on SWIR band of masked ASTER image; b) geological map of the study area as result of the integration between remote sensing analysis on ASTER images and field survey.

In conclusion, the proposed methods have proved ASTER usefulness for lithological mapping in vegetated and rough terrains with climatic and geological conditions similar to the ones of the Southern Himalayan belt (Bertoldi *et al.*, 2011).

REFERENCES

- Abrams, M. (2000): The Advanced Spaceborne Thermal Emission and Reflection Radiometer (ASTER): Data products for the high spatial resolution imager on NASA's Terra platform. *Int. J. Remote Sens.*, **21**, 847-859.
- Baldrige, A.M., Hook, S.J., Grove, C.I., Rivera, G. (2009): The ASTER spectral library version 2.0. *Remote Sens. Environ.*, **113**, 711-715.
- Bertoldi, L., Massironi, M., Visonà, D., Carosi, R., Montomoli, C., Gubert, F., Naletto, G., Pelizzo, M.G. (2011): Mapping the Buraburi granite in the Himalaya of Western Nepal: Remote sensing analysis in a collisional belt with vegetation cover and extreme variation of topography. *Remote Sens. Environ.*, **115**, 1129-1144.
- Christensen, P.R. & Harrison, S.T. (1993): Thermal Infrared emission spectroscopy of natural surfaces: Application to desert varnish coatings on rocks. *J. Geophys. Res.*, **98**, 819-834.
- Christensen, P.R., Bandfield, J.L., Hamilton, V.E., Howard, D.A., Lane, M.D., Piatek, J.L., Ruff, S.W., Stefanov, W.L. (2000): A thermal emission spectral library of rock-forming minerals. *J. Geophys. Res.*, **105**, 9735-9739.
- Clark, R.N., King, T.V.V., Klejwa, M., Swayze, G.A., Vergo, N. (1990): High spectral resolution reflectance spectroscopy of minerals. *J. Geophys. Res.*, **95**, 653-680.
- Clark, R.L., Swayze, G.A., Wise, R., Livo, K.E., Hoefen, T., Kokaly, R.F., Sutley, S.J. (2007): USGS Digital Spectral Library splib06a. *U.S.G.S. Data Ser.*, 231.
- Drury, S.A. (1997): Image interpretation in geology. London, Chapman & Hall, 283 p.
- Fujisada, H. (1995): Design and performance of ASTER instrument. In: "Advanced and next-generation satellites", H. Fujisada and M.N. Sweeting, eds. *Int. Soc. Opt. Eng.*, **2583**, 16-25.
- Hooke, R.L., Yang, H.Y., Weiblen, P.W. (1969): Desert varnish: An electron probe study. *J. Geol.*, **77**, 275-288.
- Law, R.D., Searle, M.P., Godin, L. (2006): Channel flow, ductile extrusion and exhumation in continental collision zones. *Geol. Soc. London, Spec. Pub.*, **268**, 620 pp.
- Massironi, M., Bertoldi, L., Calafà, P., Visonà, D., Bistacchi, A., Giardino, C., Schiavo, A. (2008): Interpretation and Processing of ASTER data for geological mapping and granitoids detection in the Saghro massif (eastern AntiAtlas, Morocco). *Geosphere*, **4**, 736-759.
- Nikolakopoulos, K.G., Kamaratakis, E.K., Chrysoulakis, N. (2006): SRTM vs ASTER elevation products. Comparison for two regions in Crete, Greece. *Int. J. Remote Sens.*, **27**, 4819-4838.

- Ninomiya, Y., Fu, B., Cudahy, T.J. (2005): Detecting lithology with Advanced Spaceborne Thermal Emission and Reflection Radiometer (ASTER) multispectral thermal infrared 'radiance-at-sensor' data. *Remote Sens. Environ.*, **99**, 127-139.
- Riano, D., Chuvieco, E., Salas, J., Aguado, I. (2003): Assessment of different topographic corrections in Landsat-TM data for mapping vegetation types. *IEEE Transact. Geosci. Remote Sens.*, **41**, 1056-1061.
- Rowan, L.C., Mars, J.C., Simpson, C.J. (2005): Lithologic mapping of the Mordor, NT, Australia ultramafic complex by using the Advanced Spaceborne Thermal Emission and Reflection Radiometer (ASTER). *Remote Sensing Env.*, **99**, 105-126.
- Sabins, F. (1996): Remote sensing: Principles and interpretation. New York, Freeman & Co., 494 pp.
- Salisbury, J.W. & D'Aria, D.M. (1992): Emissivity of terrestrial material in the 8-14 μm atmospheric window. *Remote Sensing Env.*, **42**, 83-106.
- Twele, A. & Erasmi, S. (2005): Optimierung der topographischen Normalisierung optischer Satellitendaten durch Einbeziehung von Kohärenzinformation. *Photogramm. Fernerk. Geoinf.*, **3**, 227-234.
- Yamaguchi, Y. & Naito, C. (2003): Spectral indices for lithologic discrimination and mapping by using the ASTER SWIR bands. *Int. J. Remote Sens.*, **24**, 4311-4323.